Available online at www.sciencedirect.com

ScienceDirect

Procedia CIRP 143 (2026) 66–69

www.elsevier.com/locate/procedia

14th CIRP Conference on Photonic Technologies

Property tailoring in multi-material Laser Directed Energy Deposition of High-Speed SynRel rotors

Chiara Gianassi[a,*], Erica Liverani[a], Andrea Cavagnino[b], Alessandro Fortunato[a]

[a]*Department of Industrial Engineering (DIN), University of Bologna, Viale del Risorgimento 2 – 40136 Bologna, Italy*
[b]*Department of Energy "G. Ferraris" (DENERG), Polytechnic of Turin, Corso Duca degli Abruzzi, 24 – 10129 Torino, Italy*

* Corresponding author. *E-mail address:* chiara.gianassi2@unibo.it

Abstract

High-speed electric motors operating up to 100 krpm are required in subsystems such as fuel cell air compressors, where rotor architectures must balance electromagnetic efficiency and mechanical robustness. This study investigates how Laser Directed Energy Deposition (L-DED) allows property tailoring in $FeSi_{2.9}$/316L bimetallic rotors by treating layer architecture as a controllable design variable. The introduction of interlayer machining further expands the design space by enabling thinner paramagnetic regions, while modifying the thermo-mechanical cycles and interfacial microstructure. Through combined mechanical testing, microhardness mapping and electromagnetic performance simulation and measurement, the relationship between process, design and properties is analyzed. Results show that thinner 316L layers increase inductance and reduce torque ripple, whereas thicker layers improve tensile performance and simplify processing. These findings demonstrate that laser-based multi-material deposition can strategically balance electromagnetic efficiency and mechanical behavior in bimetallic rotors.

Peer-review under responsibility of the scientific committee of the 14th CIRP Conference on Photonic Technologies [LANE 2026]

Keywords: Laser Directed Energy Deposition; Multi material additive manufacturing; laser processes; Synchronous Reluctance rotors; High-speed electric rotors

1. Introduction

Laser-based manufacturing technologies are gaining increasing attention in e-mobility for battery production and joining applications, where tight tolerances and complex material combinations are required [1]. In fuel cell electric vehicles, other subsystems impose similarly demanding constraints and represent promising fields for the implementation of laser processing strategies. High-speed electric compressors, which supply pressurized air to the fuel cell stack and operate above 80 000 rpm, are subjected to severe thermal, electromagnetic and mechanical loads [2], placing stringent requirements on rotor design and manufacturing. Such applications are typically addressed using permanent magnets (PM) or, more occasionally, synchronous reluctance (SynRel) rotors. PM rotors enable high rotational speeds but rely on rare-earth materials and are prone to irreversible demagnetization under current and thermal overload. Conventional SynRel rotors avoid permanent magnets, but present limited mechanical stiffness, as internal flux barriers – implemented as distributed cuts in the rotor geometry – typically restrict operational speeds below 20-30 krpm [3]. An alternative SynRel concept replaces conventional flux barriers with layers of a paramagnetic material having magnetic permeability similar to the air. Directed Energy Deposition (DED) enables the fabrication of such multi-material architectures and is therefore well suited for producing rotors composed of alternating ferromagnetic and paramagnetic layers [4]. Compared to other additive manufacturing processes, DED allows multiple independently stored feedstocks to be delivered

2212-8271 © 2026 The Authors. Published by Elsevier B.V.

Peer-review under responsibility of the scientific committee of the 14th CIRP Conference on Photonic Technologies [LANE 2026]
10.1016/j.procir.2026.07.016

through separate nozzles, avoiding changeover procedures and cross-contamination. However, its relatively low geometrical resolution makes precise layer thickness control challenging [5], which is critical since the ratio of ferromagnetic and paramagnetic regions affects electromagnetic performance. Interlayer machining has been proposed to improve dimensional accuracy in DED, although it modifies the thermo-mechanical history and may influence microstructure and residual stresses [6], [7]. In a previous work [8], a SynRel rotor based on alternating $FeSi_{2.9}$ and 316L layers was printed with FEM-optimized nominal thicknesses; nevertheless, the limitations of geometrical control in multi-material deposition have emerged, with deviations from the nominal values reaching 30%. The present study focuses on demonstrating the property tailoring potential enabled by DED in bimetallic SynRel rotors. By varying the relative fraction of ferromagnetic $FeSi_{2.9}$ and paramagnetic SS 316L – including configurations obtained through an interlayer machining to achieve very thin stainless steel regions – different material architectures were produced. Tensile tests on single-material and bimetallic specimens allowed to experimentally map the relationship between ultimate tensile strength, maximum strain and $FeSi_{2.9}$ fraction. The observed trends are interpreted in light of microstructural evolution and hardness variations induced by the different thermo-mechanical histories. The electromagnetic behavior of the rotors was initially determined by comparing finite element simulations of two motor prototypes designed to operate nominally at 100 krpm and 100 mNm. Preliminary experiments, limited to 50 krpm due to hardware limitations, confirm that differences can be observed in the two motor designs. Results demonstrate that DED-printed bimetallic rotors are not only a proof of concept, but a tailorable design solution in which layer architecture and processing strategy can be adjusted to balance electromagnetic and mechanical performance.

2. Materials and methods

The bimetallic and single-material preforms were printed on 316L substrate using gas atomized powders: a ferromagnetic iron-silicon alloy ($FeSi_{2.9}$, 45-106 µm) and a paramagnetic austenitic stainless steel (SS 316L, 53-150 µm). Chemical compositions are reported in Table 1. The Directed Energy Deposition system was equipped with a Laserline LDF-4500-60 diode laser with a maximum power of 4.5 kW. The optical setup included Laserline OTS-5 focusing optics with a collimation length of 80 mm and a focal length of 300 mm, resulting in a spot diameter of 2.2 mm. The GTV PN6625 coaxial nozzle features six outlets: three connected to the $FeSi_{2.9}$ powder hopper and three to the 316L hopper (Fig. 1a), enabling independent material feeding. Further details on L-DED configuration and process parameters adopted are included in [8]. The layer distributions of the bimetallic rotors (Fig. 1b) derived from two rotor designs previously optimized through finite element electromagnetic simulations under different constraints [9]. As a consequence, the relative fraction of ferromagnetic and paramagnetic material varied. Interlayer machining was applied only in the second preform to obtain thinner 316L regions, increase the FeSi content and therefore the rotor inductance. Both preforms were subjected to annealing at 850°C for 1 hour. Tensile specimens were extracted from the central region of each rotor blank. The resulting specimens exhibited $FeSi_{2.9}$ fractions of 0, 28, 34, 60, 65 and 100% within the load-bearing cross section (Fig. 1c). The $FeSi_{2.9}$ percentage in each specimen was determined experimentally by analyzing polished cross-sections and confirmed by SEM-EDS elemental mapping. EDS analyses were performed at an accelerating voltage of 12 kV and a working distance of 24.4 mm using a Bruker X Flash 630 M. Elemental quantification was carried out using a standardless ZAF correction. Tensile specimens were tested according to BS EN ISO 6892 using a gauge length of 25 mm. Microhardness measurements (ISO 6507–1:2023) were carried out along the build direction with a spacing of 150 µm between indentation and 0.2 kg load.

Table 1. Chemical composition of the powders evaluated through SEM-EDS

[wt%]	Fe	Si	Cr	Mn	Ni	Mo
AISI 316L	bal.	1.15	17.21	1.65	10.55	2.39
$FeSi_{2.9}$	bal.	3.36	-	-	-	-

Electromagnetic characterization was performed on a dedicated high-speed test bench. The rotor was assembled into a 2-pole 3-phase stator (Fig. 1d) and powered by a SiC-based three-level PWM inverter, operating at a DC bus voltage of 530 V and a switching frequency of 40 kHz. The motor was controlled with a maximum torque ampere strategy.

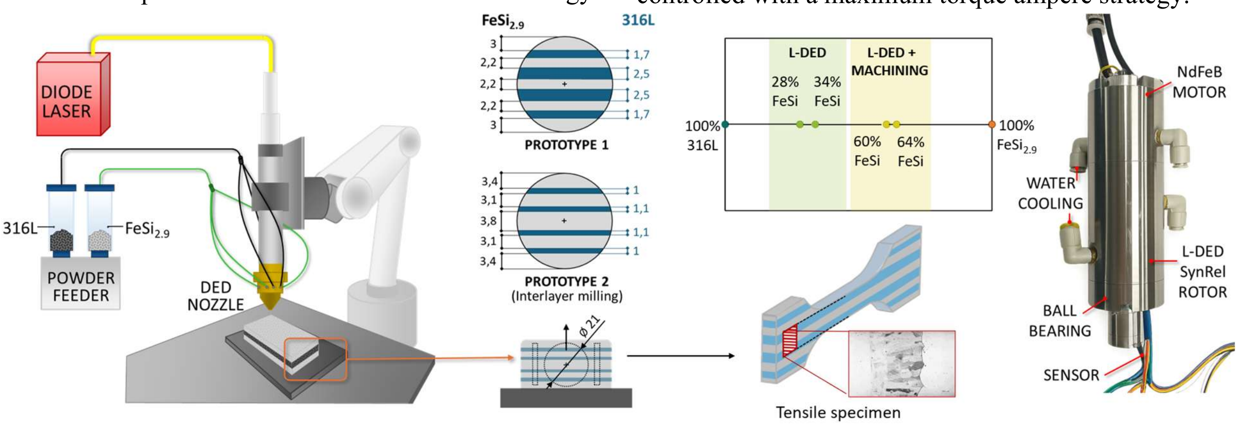

(a) (b) (c) (d)

Fig. 1. (a) Schematic of DED setup with alternating deposition of $FeSi_{2.9}$ and 316L; (b) layer thickness distribution in the bimetallic rotor blanks for prototype 1 (L-DED only) and prototype 2 (DED + interlayer machining); (c) geometry of a tensile specimen showing build direction, layer orientation and $FeSi_{2.9}$ fractions; (d) motor test bench for electromagnetic performance

Inductance maps were experimentally obtained by acquiring phase voltages and currents in the synchronous (d, q) reference frame at torque levels up to 150 mNm and low rotational speeds (15-20 krpm) to reduce the impact of iron core losses on results.

3. Results and discussions

3.1. Mechanical and microstructural response

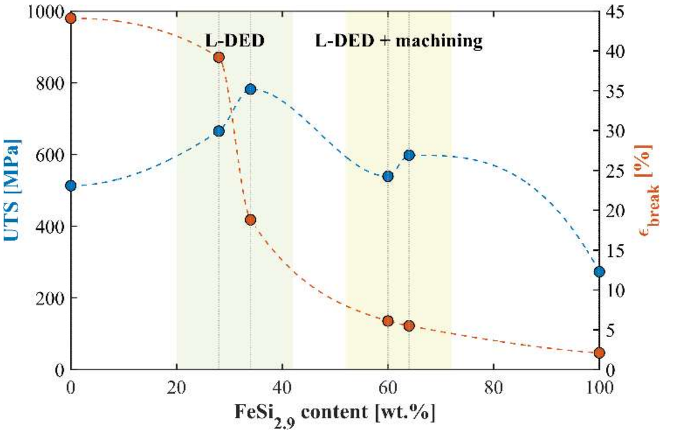

Fig.2. Ultimate tensile strength (left axis) and strain at break (right axis) as a function of the $FeSi_{2.9}$ fraction in the specimen cross section.

Figure 2 reports the ultimate tensile strength (UTS) and maximum strain obtained from tensile tests as a function of the $FeSi_{2.9}$ content; the remaining fraction corresponds to austenitic stainless steel 316L. Previous single-material tensile tests highlighted the brittle behavior of L-DED printed $FeSi_{2.9}$ and the ductile response of 316L, characterized by high elongation values and dimples on the fracture surfaces. Although the bimetallic specimens are expected to exhibit an intermediate mechanical response between the two constituent alloys, this assumption holds true only for elongation, while UTS values consistently exceed those of both monolithic materials, suggesting that the layered structures promote strengthening mechanisms. Regarding fracture behavior, the $FeSi_{2.9}$ layers retain their brittle nature, while the 316L layers maintain ductile characteristics; the layered morphology remains clearly distinguishable on the fracture surfaces. For specimens containing lower $FeSi_{2.9}$ fractions (up to 34%) and produced without interlayer machining, 316L acts as a continuous matrix while FeSi behaves as a reinforcing phase. At higher iron-silicon fractions, the tensile strength increases and the maximum strain decreases. The higher UTS is consistent with effective load transfer between layers and indicates good interfacial bonding. At 34% $FeSi_{2.9}$, the maximum UTS of 782 MPa is recorded, accompanied by a significant reduction in strain associated to the brittle FeSi phase. Specimens produced with interlayer machining are characterized by a dominant $FeSi_{2.9}$ fraction (60-64%). Maximum strain values range between 5-6%, while UTS remains higher than that of the iron-silicon. This indicates that local reinforcement mechanisms still contribute to enhanced tensile strength. Metallurgical features contributed to further interpret the tensile results. Figure 3 compares cross sections extracted from the two prototypes and their microhardness, highlighting the $FeSi_{2.9}$ grain morphology. In the first prototype, $FeSi_{2.9}$ exhibits large columnar grains, resulting from progressive thermal accumulation during layer-by-layer deposition. Conversely, in the specimen with interlayer machining, grain size is smaller in the first deposited layers and progressively increases in subsequent layers, eventually recovering a columnar morphology. This difference is attributed to the altered thermal cycle, since material deposition after each milling step occurs on a surface at room temperature, therefore the initial layers experience higher cooling rates, limiting grain growth. This phenomenon affects also the magnetic performance, since grain boundaries hinder demagnetization. In samples produced without interlayer machining, hardness remains relatively constant within the individual layers, with average values of 219 HV for 316L and 232 HV for $FeSi_{2.9}$. At the interfaces, however, hardness increases reaching an average of 357 HV. For example, the layer identified as “T1” in Figure 3 has a chemical composition corresponding to $FeSi_{2.9}$, yet the abrupt hardness increase suggests the formation of intermetallic compounds, as confirmed by XRD analysis [8]. Specimen produced with interlayer machining shows an average microhardness of 222 HV for 316L and 214 HV for $FeSi_{2.9}$. The overall trend remains similar, with localized peaks at the interfaces, but the transition zones are thinner due to the milling step and the peak hardness values are lower, with an average of 297 HV. This reduced interfacial hardness is consistent with the lower tensile strengths measured in these configurations.

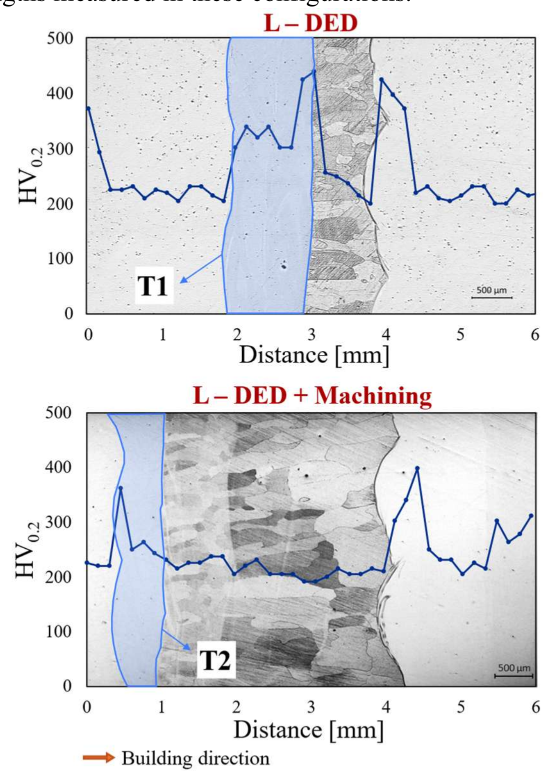

Fig. 3. Microhardness profiles along the build direction. “T1” and “T2” denote the transition zones between $FeSi_{2.9}$ and 316L.

3.2. Electromagnetic response

The first motor prototype was designed and built to prove the feasibility of printing axial laminated anisotropic rotors using L-DED. During geometry qualification, it was found that the specified layer thicknesses and their positioning with respect to the rotational axis were fairly respected due to the low print resolution of DED. However, Table 2 shows that the differences between design and prototype 1 are minimal (with the exception of the torque ripple), leading to conclude that interlayer machining can be avoided for layer thicknesses above approximately 2 mm. This value, however, is specific to the adopted DED setup, as it depends on the laser spot size and the minimum achievable build height per single pass. The second prototype was designed to minimize losses and torque ripple. The electromagnetic optimization led to very thin 316L layers, making the interlayer machining necessary to obtain the wanted layer thicknesses. In the second prototype, the significant torque ripple reduction has been obtained at the cost of a higher supply voltage due to the higher $FeSi_{2.9}$ volumetric fraction and spatial distribution of the ferromagnetic material within the rotor cross section. The measurements executed at rotational speed of 20 and 50 krpm with rated torque of 100 mNm also prove that the prototype 2 shows a slightly lower phase current and higher estimated efficiency at both speeds compared to the original one (Table 3). Due to its bigger inductances, the second prototype requires higher supply voltage to inject the needed current to generate the torque. At the end, comparing simulations and measurement obtained from testing (Tables 2, 3) it seems that the simplified modeling assumptions – mainly on material permeability and effective anisotropy – may have introduced conservative estimations.

Table 2. FEM results at 100 krpm and 100 mNm (45° current angle). Prototype 2 (with interlayer machining) shows a single dataset, as nominal and manufactured geometries coincide

	Design 1	Prototype 1	Design & Protoype 2
Phase current *(A_{rms})*	2.94	3.05	2.96
Phase voltage *(V_{rms})*	211.4	213.5	234.1
Power factor	0.60	0.58	0.54
Phase resistance @115 *(Ω)*	1.90	1.90	1.82
d-axis inductance *(mH)*	9.50	8.83	10.31
q-axis inductance *(mH)*	1.75	1.64	2.68
Salient ratio *(-)*	5.44	5.39	3.85
Torque ripple *(mNm)*	30	131	22
Tot. electromagnetic losses *(W)*	257	259	238
Electromagnetic efficiency *(%)*	80.3	80.2	81.5

Table 3. Measurement results for the Prototype 1 (P1) and Prototype 2 (P2)

Test conditions (V_{bus} = 530 V_{DC}, $f_{switching}$ = 40 kHz, star connected)				
Speed *(rpm)*	**25000**		**50000**	
Frequency *(Hz)*	417		833	
Estimated torque *(Nm)*	0.1		0.1	
Estimated shaft power *(W)*	261.8		523.6	
Steady state thermal test (thermal time with active cooling ≈ 3 minutes)				
	P1	**P2**	**P1**	**P2**
Full spectrum, line-to-line voltage *(V)*	151.4	159.3	208.8	239.7
Full spectrum, phase current *(A)*	3.540	3.347	3.545	3.440
Full spectrum input power *(W)*	362.4	343.3	662.4	663.1
Estimated total losses *(W)*	100.6	81.5	138.8	139.5
Estimated efficiency *(%)*	72.2	76.3	79.0	79.0

4. Conclusions

High-speed bimetallic SynRel rotors have the potential to become a realistic and tunable design solution for demanding applications. With the multi-material approach allowed by Directed Energy Deposition it is possible to make layers architecture a design variable. The introduction of interlayer milling significantly expands the design space. By removing material between deposition steps, tighter control of layer thickness is achieved, enabling thinner 316L flux barriers and, consequently, a higher relative $FeSi_{2.9}$ fraction within the rotor cross section. This modification improves control over electromagnetic anisotropy and reduces torque ripple and rotor losses, as demonstrated in previous optimization analyses. At fixed operating conditions (100 krpm, 100 mNm) and constant rotor dimensions, different performance priorities can be addressed through layer thickness selection. When mechanical properties are the main objective, thicker 316L layers are required to ensure process stability and geometric robustness. This configuration results in a higher overall ductile fraction, with improved tensile strength and maximum strain, a simpler and faster manufacturing route, and reduced microstructural heterogeneity at the interfaces. However, the increased paramagnetic fraction lowers the d-axis inductance and introduces greater sensitivity to layer growth deviations. Conversely, thinner 316L layers (below ~2 mm in our system) can be introduced to increase the relative $FeSi_{2.9}$ fraction and inductance, therefore reducing torque ripple and rotor losses. Achieving such geometries requires interlayer machining. At the same time, it modifies the thermo-mechanical cycle, promotes interfacial grain refinement, slightly reduces tensile properties, and increases processing time. Overall, the combination of material selection, layer thickness design, and optional interlayer machining allows to control the trade-off between electromagnetic efficiency and mechanical robustness.

Acknowledgements

This study was carried out within the «TUrBO: the next 100,000+rpm synchronous reluctance motor drives» project – funded by European Union – Next Generation EU within the PRIN 2022 program (D.D. 104 - 02/02/2022 Ministero dell'Università e della Ricerca).

References

[1] A. G. Demir *et al.*, «Challenges and Opportunities for Laser Applications in Electric Vehicle Manufacturing», in *Selected Topics in Manufacturing*, L. Carrino, L. M. Galantucci, e L. Settineri, A c. di, in Lecture Notes in Mechanical Engineering. , Cham: Springer Nature Switzerland, 2024, pp. 219–253. doi: 10.1007/978-3-031-41163-2_12.

[2] D. Fodorean, «High-Speed Electric Motors for Fuel Cell Compressor System Used for EV Application—Review and Perspectives», *Applied Sciences*, vol. 16, fasc. 1, p. 476, gen. 2026, doi: 10.3390/app16010476.

[3] M. Murataliyev, M. Degano, M. Di Nardo, N. Bianchi, e C. Gerada, «Synchronous Reluctance Machines: A Comprehensive Review and Technology Comparison», *Proc. IEEE*, vol. 110, fasc. 3, pp. 382–399, mar. 2022, doi: 10.1109/JPROC.2022.3145662.

[4] Y. Cui, C. Gianassi, A. Fortunato, L. Zarri, e A. Cavagnino, «High-Speed Synchronous Reluctance Motors with Additively Manufactured Rotors».

[5] D. R. Feenstra, R. Banerjee, H. L. Fraser, A. Huang, A. Molotnikov, e N. Birbilis, «Critical review of the state of the art in multi-material fabrication via directed energy deposition», *Current Opinion in Solid State and Materials Science*, vol. 25, fasc. 4, p. 100924, ago. 2021, doi: 10.1016/j.cossms.2021.100924.

[6] S. Sadeh *et al.*, «Interlayer machining effects on microstructure and residual stress in directed energy deposition of stainless steel 316L», *Journal of Manufacturing Processes*, vol. 94, pp. 69–78, mag. 2023, doi: 10.1016/j.jmapro.2023.03.036.

[7] P. Li, Y. Gong, Y. Xu, Y. Qi, Y. Sun, e H. Zhang, «Inconel-steel functionally bimetal materials by hybrid directed energy deposition and thermal milling: Microstructure and mechanical properties», *Archives of Civil and Mechanical Engineering*, vol. 19, fasc. 3, pp. 820–831, mag. 2019, doi: 10.1016/j.acme.2019.03.002.

[8] C. Gianassi *et al.*, «Laser directed energy deposition of FeSi/SS 316L advanced bimetallic high-speed rotors: From material characterization to performance evaluation», *Advances in Industrial and Manufacturing Engineering*, vol. 11, p. 100175, nov. 2025, doi: 10.1016/j.aime.2025.100175.

[9] Y. Cui, C. Gianassi, G. Rizzoli, A. Fortunato, L. Zarri, e A. Cavagnino, «Prototyping and Optimization of 100,000 rpm Additively Manufactured SyR Rotors», in *2025 IEEE Energy Conversion Conference Congress and Exposition (ECCE)*, Philadelphia, PA, USA: IEEE, ott. 2025, pp. 1–7. doi: 10.1109/ECCE58356.2025.11259600.